Tuning hydrophobic composition in terpolymer-based anion exchange membranes to balance conductivity and stability

Journal:	*Molecular Systems Design & Engineering*
Manuscript ID	ME-ART-02-2022-000027.R1
Article Type:	Paper
Date Submitted by the Author:	09-Mar-2022
Complete List of Authors:	Ozawa, Yoshihiro; University of Yamanashi, Clean Energy Research Shirase, Yuto; University of Yamanashi, Clean Energy Research Otsuji, Kanji; University of Yamanashi, Clean Energy Research Center Miyatake, Kenji; University of Yamanashi, Clean Energy Research

As next-generation fuel cells, anion exchange membrane fuel cells (AEMFCs) have attracted considerable attention because of high energy conversion efficiency, zero-emission, and possible use of non-precious metal eletrocatalysts. One of the most critical issues in AEMFCs is insufficient properties and durability of AEMs. The difficulties lie in the fact that the hydroxide ion conductivity and chemical/physical stability are in trade-off relationship. In order to address this issue, we focus on novel terpolymer-based AEMs in the present study, where composition of the hydrophobic components (hexafluoroisopropylidene and perfluorohexylene groups) was investigated in detail. We found that the membrane exhibited volcano-type dependence of the conductivity on the hydrophobic composition and that very high conductivity was achieved with the optimized composition. AMEFC test verified the advantages of the resulting AEMs.

Tuning hydrophobic composition in terpolymer-based anion exchange membranes to balance conductivity and stability

Yoshihiro Ozawa,[a] Yuto Shirase,[a] Kanji Otsuji,[a] Kenji Miyatake*[b,c,d]

[a]Interdisciplinary Graduate School of Medicine and Engineering, University of Yamanashi, 4 Takeda, Kofu, Yamanashi 400-8510, Japan

[b]Fuel Cell Nanomaterials Center, University of Yamanashi, 6-43 Miyamae-cho, Kofu 400-0021, Japan

[c]Clean Energy Research Center, University of Yamanashi, 4 Takeda, Kofu, Yamanashi 400-8510, Japan

[d]Department of Applied Chemistry, Waseda University, Tokyo 169-8555, Japan

*Corresponding author

E-mail addresses: miyatake@yamanashi.ac.jp (K. Miyatake)

Keywords: anion exchange membranes, ionomers, alkaline fuel cells

ABSTRACT

We designed and synthesized novel terpolymer-based anion conductive polymers, where the effect of hydrophobic composition on membrane properties was investigated in details. Precursor terpolymers were first prepared from 2,2-bis(4-chlorophenyl)hexafluoropropane (BAF), 1,6-bis(3-chlorophenyl)perfluorohexane (PAF), and 2,7-dichloro-9,9-bis[6'-(N,N-dimethylamino)hexyl]fluorene via Ni(0)-promoted polycondensation reaction. The following quaternization reaction with dimethyl sulfate was successful to obtain five terpolymers, QBPA with different PAF/(BAF+PAF) compositions and supposed chemical structure. The QBPA provided thin and bendable membranes by solution casting. TEM images suggested that the membranes exhibited phase-separated morphology similar to those of the corresponding parent copolymer membranes. SAXS profiles indicated that QBPA-4 containing 83 mol% PAF exhibited the most distinct periodic structure based on the hydrophobic component. The hydroxide ion conductivity of the membranes showed a volcano-type dependence on the hydrophobic composition, and the highest conductivity (161 mS cm^{-1}) was achieved with QBPA-1 membrane at 80 ºC. Taking also the other properties into account, QBPA-1 and QBPA-5 containing 17 mol% PAF seemed the best-balanced membranes. Alkaline fuel cell using the QBPA-1 membrane achieved the maximum power density of 273 mW cm^{-2}, exceeding that using the copolymer BAF-QAF membrane (185 mW cm^{-2}).

Introduction

Fuel cells and water electrolysis devices have become more and more important toward the realization of hydrogen-based sustainable society. In particular, alkaline fuel cells and water electrolysis using anion exchange membranes (AEMs) are expected to play pivotal roles because of high energy conversion efficiency and possible use of non-noble metal electrocatalysts, compared to the acidic equivalents that are presently commercialized. Their performance has been significantly improved through the extensive research work in the last decade, however, durability still does not meet the requirements mostly because of the chemical/physical degradation of AEMs and electrocatalysts as major constituent materials.[1,2]

Typical AEMs are composed of polymer backbone and cationic head groups with counter hydroxide ions. Benzyl trimethylammonium groups have been most used due to the synthetic reason.[3] For example, poly(arylene ether sulfone) block copolymers containing benzyltrimethylammonium cation achieved very high hydroxide ion conductivity of 209 mS cm^{-1} at 100 ℃ and 100% relative humidity (RH).[4] Wang et al. introduced pendant ammonium groups densely onto low-density polyethylene to achieve similarly high hydroxide ion conductivity of 208 mS cm^{-1} at 80 ℃ and 100% RH.[5] However, they experience degradation via nucleophilic attack of the hydroxide ions under the alkaline conditions. Therefore, other cationic groups such as imidazolium and phosphonium groups

have also been investigated.[6,7] Poly(phenylene ether) tethered with six-membered heterocyclic 6-azonia-spiro [5.5] undecane (ASU) survived in 1 M NaOH/H_2O at 80 ℃ for 1500 h.[8] However, the nucleophilic reaction of the hydroxide ions takes place not only on the ionic groups but also on the polymer main chain (in particular, arylene ether groups), which can cause hydrolysis of the main chain and eventual mechanical failure of the membranes. [9,10] Therefore, ether-free polymer main chain seems indispensable for alkaline stable AEMs. Poly(bis-arylimidazolium)s with different side chain length maintained more than 90% imidazolium groups in 10 M KOH at 80 ℃ for 240 h.[11] It was claimed that the steric hindrance around the cationic groups mitigated the nucleophilic reaction.

With regard to the hydroxide ion conductivity, the focus has been on maximizing the ion exchange capacity (IEC) and constructing proper ion-transporting pathway, while balancing the above-mentioned chemical stability.[12,13] Chen et al. reported that cross-linked poly(norbornene) had excellent ion conductivity of 195 mS cm^{-1} at 80 ℃ and alkaline stability over 500 h in 1 M NaOH at 80 ℃, however, that the membranes were not mechanically tough with low elongation at fracture point (less than ca. 50%) and low tensile stress.[14] Those previous works indicate that the alkaline stability and ion conductivity were adjustable by changing the cationic groups, nearby substituents, and the polymer main chains. In most cases, however, mechanical strength of the resulting AEMs was insufficient or the

effect of those structural modifications on mechanical properties (e.g., Young's modulus and elongation at break point) has not been well-understood.

In the pursuit of more ion conductive and chemically and mechanically durable AEMs, we developed a series of quaternized copolymers containing pendant trimethylammonium groups and fluorinated aliphatic or aromatic groups.[15] The characteristic features of those AEMs were that fluorenyl groups served as a scaffold for hexyl trimethylammonium head groups to have high local ionic density while highly hydrophobic nature of the fluorinated components contributed to the well-developed morphology and the formation of ionic channels. Lack of heteroatom linkages in the main chain provided the resulting membranes with high alkaline stability. Perfluoroalkylene (PAF) groups were also effective in improving the mechanical properties. In fact, QPAF-4 membranes containing perfluorohexylene groups in the main chain achieved high elongation at break (ca. 200%) promising for practical applications.[16] Hexafluoroisopyridene (BAF) groups, in contrast, had an effect to suppress excessive swelling (or water absorption) for high IEC BAF-QAF membranes, resulting in high hydroxide ion conductivity (134 mS cm^{-1} in water at 80 ºC).[17]

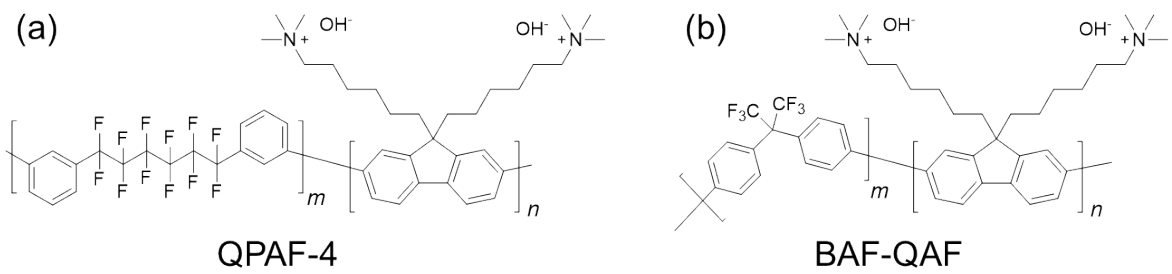

QPAF-4 BAF-QAF

Fig. 1 Chemical structures of (a) QPAF-4 and (b) BAF-QAF membranes.

The objective of the present study is to design and synthesize terpolymer-based AEMs employing both PAF and BAF components and to elucidate the effect of the hydrophobic composition on the membrane properties. Phase-separated morphology, hydroxide ion conductivity, water absorbability, mechanical strength, gas permeability, and alkaline stability were investigated in details and discussed as a function of the hydrophobic composition. A selected membrane with tuned structure and balanced properties was subjected to alkaline fuel cell evaluation.

Experimental

Materials

2,2-Bis(4-aminophenyl)hexafluoropropane (> 97.0%, FUJIFILM Wako Pure Chemical), sodium nitrite (> 98.5%, Kanto Chemical), copper(II) sulfate pentahydrate (> 99.5%, Kanto Chemical), sodium hydrogen sulfate (> 58.5%, Kanto Chemical), sodium chloride (> 99.0%, Kanto Chemical), 3-iodoaniline (> 96%, Combi-Blocks), 1,6-diiodoperfluorohexane (Tosoh Fine Chem.), copper, powder (> 99.5%, Kanto Chemical), dimethyl sulfoxide (DMSO) (> 99.0%, Kanto Chemical), ethyl acetate (AcOEt) (> 99.3%, Kanto Chemical), dichloromethane (CH_2Cl_2) (> 99.0%, Kanto Chemical), hexane (> 95.0%, Kanto Chemical),

sodium sulfate (> 98.5%, Kanto Chemical), potassium carbonate (> 99.5%, Kanto Chemical), hydrochloric acid (35-37%, Kanto Chemical), potassium hydroxide (> 86.0%, Kanto Chemical), 2,2'-bipyridyl (> 99.0%, TCI), bis(1,5-cyclooctadiene)nickel(0) ($Ni(COD)_2$) (> 95.0%, Kanto Chemical), and dimethyl sulfate (> 99%, Kanto Chemical) were used as received. N,N-Dimethylacetamide (DMAc) (> 99.0%, Kanto Chemical) was purified with a solvent refining apparatus before use. Monomer **3** was synthesized according to the literature.[11]

2,2-Bis(4-chlorophenyl)hexafluoropropane (monomer 1) (Scheme 1)

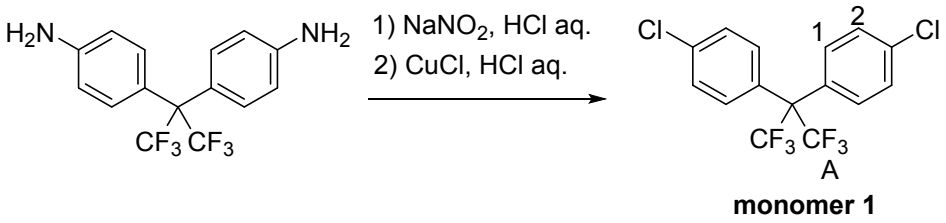

Scheme 1 Synthesis of monomer **1**.

2,2-Bis(4-aminophenyl)hexafluoropropane (5.00 g, 14.96 mmol) was dissolved in 8 M HCl aq. (40 mL) in a 100 mL round-bottom flask in an ice bath. A solution of $NaNO_2$ (3.09 g, 44.88 mmol) in 10 mL of water was added dropwise by pipette to the mixture with stirring. The resulting slurry was stirred for 30 min in an ice bath. The mixture was added dropwise by pipette to a solution of CuCl (5.92 g, 59.83 mmol) in 15 mL of conc. hydrochloric acid with stirring. The mixture was reacted for 1.5 h at rt. The reaction was quenched by the addition of 2.5 M K_2CO_3 aq. (100 mL). The precipitate was collected by filtration. The crude

product was purified by column chromatography on silica gel (eluent: hexane) to obtain the monomer **1** as a white powder (2.62 g) in 47% yield.

1,6-Bis(3-chlorophenyl)perfluorohexane (monomer 2) (Scheme 2)

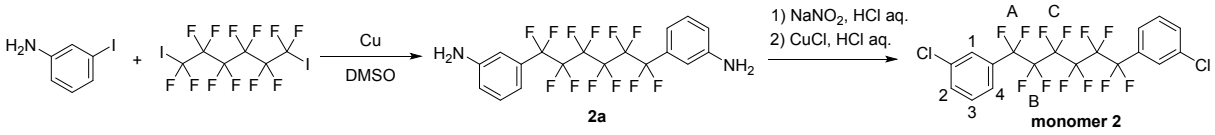

Scheme 2 Synthesis of monomer **2**.

2a. A mixture of 3-iodoaniline (10.0 g, 36.20 mmol) and copper (5.43 g, 90.50 mmol) in 26mL of degassed DMSO were stirred at 100 °C with a nitrogen balloon. To the mixture, a solution of 1,6-diiodoperfluorohexane (10.0 g, 18.10 mmol) in 6 mL of degassed DMSO was added slowly and the mixture was stirred for 24 h at 100 °C. The reaction was quenched by the addition of deionized water (20ml). The mixture was filtered to remove water. The precipitate was dissolved in ethyl acetate and filtered to remove the cuprous salts. The filtrate was washed with brine several times. The organic layer was dried over Na_2SO_4 with activated carbon, filtered, and evaporated under vacuum. The resulting oily product was purified by column chromatography on silica gel (eluent: CH_2Cl_2) to obtain **2a** as a pale yellow powder (6.85 g) in 59% yield.

Monomer 2. To a solution of **2a** (4.00 g, 8.25 mmol) in 8 M HCl aq. (42 mL) in an ice bath was added dropwise 3 mL of 6.3 M $NaNO_2$ aq. The mixture was stirred for 1 h and added to a mixture of CuCl (2.50 g, 25.03 mmol) and conc. hydrochloric acid (10 mL) cooled at 0 °C.

After stirred for 1.5 h at 0 °C, the reaction mixture was poured into 100 mL of 2.5 M K_2CO_3 aq. The mixture was filtered through a Celite plug. The aqueous layer was extracted with ethyl acetate and the combined organic layer was dried over Na_2SO_4, filtered, and evaporated under reduced pressure. The residue was purified by column chromatography on silica gel (eluent: hexane) to obtain **2** as a pale yellow powder (1.91 g) in 44% yield.

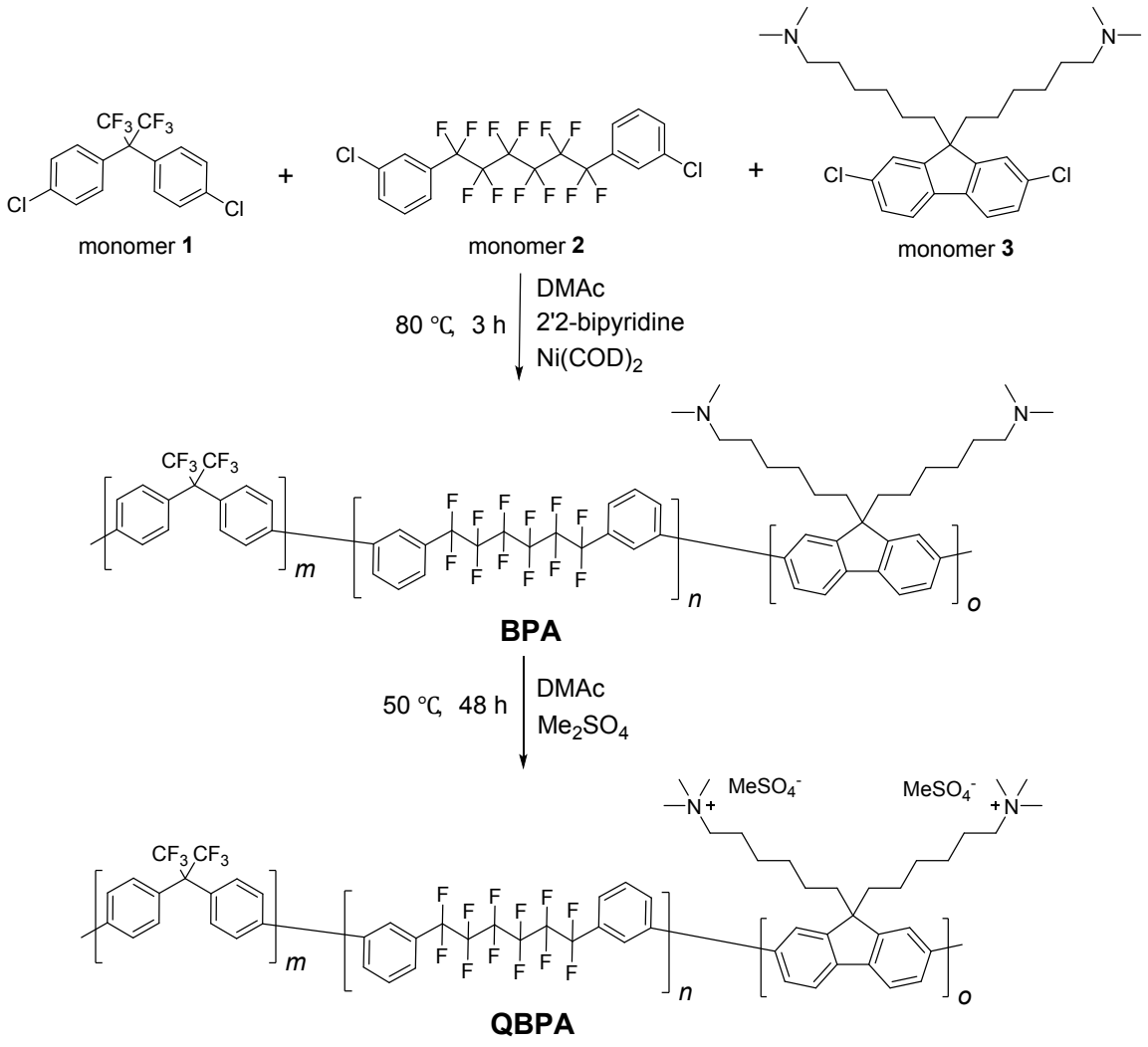

Scheme 3 Synthesis of QBPA.

Polymerization

A typical procedure is as follows (Scheme 3). A 100 mL three-necked flask equipped with a nitrogen inlet and a mechanical stirrer was charged with **1** (0.700 g, 1.88 mmol), **2** (0.210 g, 0.38 mmol), **3** (0.780 g, 1.59 mmol), 2,2'-bipyridyl (3.07 g, 19.70 mmol), and DMAc (13 mL). The mixture was heated at 80 ºC to obtain a homogeneous mixture. To the mixture, $Ni(COD)_2$ (3.00 g, 10.90 mmol) was added. After the polymerization for 3 h, the mixture was poured into a mixture of methanol and conc. hydrochloric acid (1:5 by volume, 300 mL) to precipitate a black fibrous solid. The crude product was washed with concentrated hydrochloric acid (200 mL) and then treated with 0.1 M potassium carbonate aqueous solution (200 mL). The pale yellow product was washed with deionized water (200 mL) and dried at 50 ºC in a vacuum oven to obtain 1.40 g of BPA (*m*1.00*n*0.20*o*0.84) as a yellow fibrous solid in 100% yield. BPA of other compositions were obtained by the similar procedure.

Quaternization of QBPA terpolymers

A typical procedure is as follows. A 100 mL round-bottomed flask was charged with BPA (*m*1.00*n*0.20*o*0.84) (1.24 g, 6.79 mmol of dimethylamino groups) and DMAc (20 mL). After dissolution of the polymer, dimethyl sulfate (6.44 mL, 67.90 mmol) was added. The mixture was stirred for 48 h at 50 ºC. After quaternization of the polymer, the mixture was poured into deionized water (200 mL) to precipitate a yellow fibrous solid. The product was washed

with deionized water (200 mL) and dried at 50 ºC in a vacuum oven to obtain 1.52 g of QBPA (*m*1.00*n*0.20*o*0.84) as a yellow fibrous solid in 96% yield. QBPA of other compositions were obtained by the same procedure.

Preparation of QBPA membranes

The quaternized terpolymer was dissolved with DMAc (10 mL) and filtered with a syringe stuffed with cotton. The filtrate was cast onto a flat glass plate. Drying the solution at 50 ºC overnight gave a transparent light brown membrane (ca. 50 μm thick). The counter anion was exchanged to hydroxide ion by soaking the membrane in 1 M KOH aq. at 80 ºC for 48 h. The resulting membrane was washed and immersed in degassed, deionized water at least for 1 d to ensure complete removal of excess KOH. QBPA in chloride ion form was prepared treating the membrane in hydroxide ion form with 1 M hydrochloric acid for 48 h at rt.

Preparation of membrane electrode assembly (MEA) and fuel cell operation

An MEA was prepared by a slightly modified method from the previously reported procedure,[17] using QBPA-1 as the electrolyte membrane and QPAF-4 as the electrode binder. The catalyst inks for the anode and cathode were prepared with Pt catalyst supported on carbon black (Pt/CB: TEC10E50E, Tanaka Kikinzoku Kogyo, K. K.), methanol and pure water by stirring for 30 min in a planetary ball mill containing 20 zirconia beads with a diameter of 5 mm. 5 wt% QPAF-4 (IEC = 2.06 meq g^{-1}) in methanol solution was added to the slurry, and the mixture was further stirred in a planetary ball mill for 30 min. The weight

ratio of the QPAF-4 binder to the catalyst was set to 0.43. These catalyst inks were directly sprayed onto the microporous layers (MPLs) of the gas diffusion layers (GDLs) for the anode (W1S1010, Cetech Co., Ltd.) and cathode (29BC, SGL Carbon Group Co., Ltd.), respectively, by the pulse-swirl-spray (PSS, Nordson Co., Ltd.) technique to prepare the gas diffusion electrodes (GDEs). The electrode area was 4.41 cm^2, and the Pt loading was ca. 0.20 mg_{Pt} cm^{-2} for both electrodes. The prepared GDEs were immersed in 1 M KOH at 80 ºC for 2 days to ion-exchange to the OH^- form. Similarly, the QBPA-1 electrolyte membrane (IEC = 2.11 meq. g^{-1}, ca. 30 μm thick) was also immersed in 1 M KOH aqueous solution at 80 °C for 2 days. Surface KOH solution on the GDEs and the electrolyte membrane were wiped with Kim Towels (Nippon Paper Cresia Co., Ltd.). The GDEs and the electrolyte membrane were immersed in ultrapure water for ca. 1 h, and then wiped with Kim Towels again to remove the ultrapure water. QBPA-1 membrane was sandwiched with two GDEs and pressed in a single cell without heating. The resulting MEA was sandwiched between two graphite flow plates and 200 μm silicone/poly(ethyl benzene-1, 4-dicarboxylat/silicone gaskets (SB50A1P, Maxell Kureha Co., Ltd.), and fastened at 10 kgf cm^{-2} with four springs. A fuel cell with the MEA was operated at 60 ºC supplying humidified hydrogen (100% RH) to the anode at a flow rate of 100 mL min^{-1} and humidified oxygen (100% RH) to the cathode at a flow rate of 100 mL min^{-1}, respectively. Serpentine and comb-shaped flow fields were used for the anode and the cathode, respectively.

Results and Discussion

Synthesis of QBPA terpolymers

Precursor BPA terpolymers were synthesized by the polymerization of monomers **1**, **2**, and **3** in the presence of bis(1,5-cyclooctadiene)nickel(0) ($Ni(COD)_2$) (Scheme 4). The feed composition of the hydrophobic monomers **1** and **2** was changed from n/(m+n) = 0.17-0.83, while the target ion exchange capacity (IEC) of the resulting quaternized terpolymers was set at 2.10 (Nos. 1-4) or 2.50 (No. 5) meq. g^{-1}. The polymerization reaction proceeded well to give the BPA terpolymers in quantitative yields (Table 1). The obtained polymers were soluble in chloroform, DMSO, and DMAc. The structure of BPA terpolymers was analyzed by ^{1}H and ^{19}F NMR spectra. A typical example is shown in Fig. 2 for BPA-1 (m/n/o=1.00/0.20/0.84), where all proton and fluorine peaks were well-assigned to the supposed structure. From the integral of the proton peaks, the experimental compositions were estimated, which were in fair agreement with those of the feed compositions. The molecular weight of the BPA terpolymers was M_n = 7.1-9.4 and M_w = 35.2-56.4 with reasonable polydispersity M_w/M_n = 4.9-6.0.

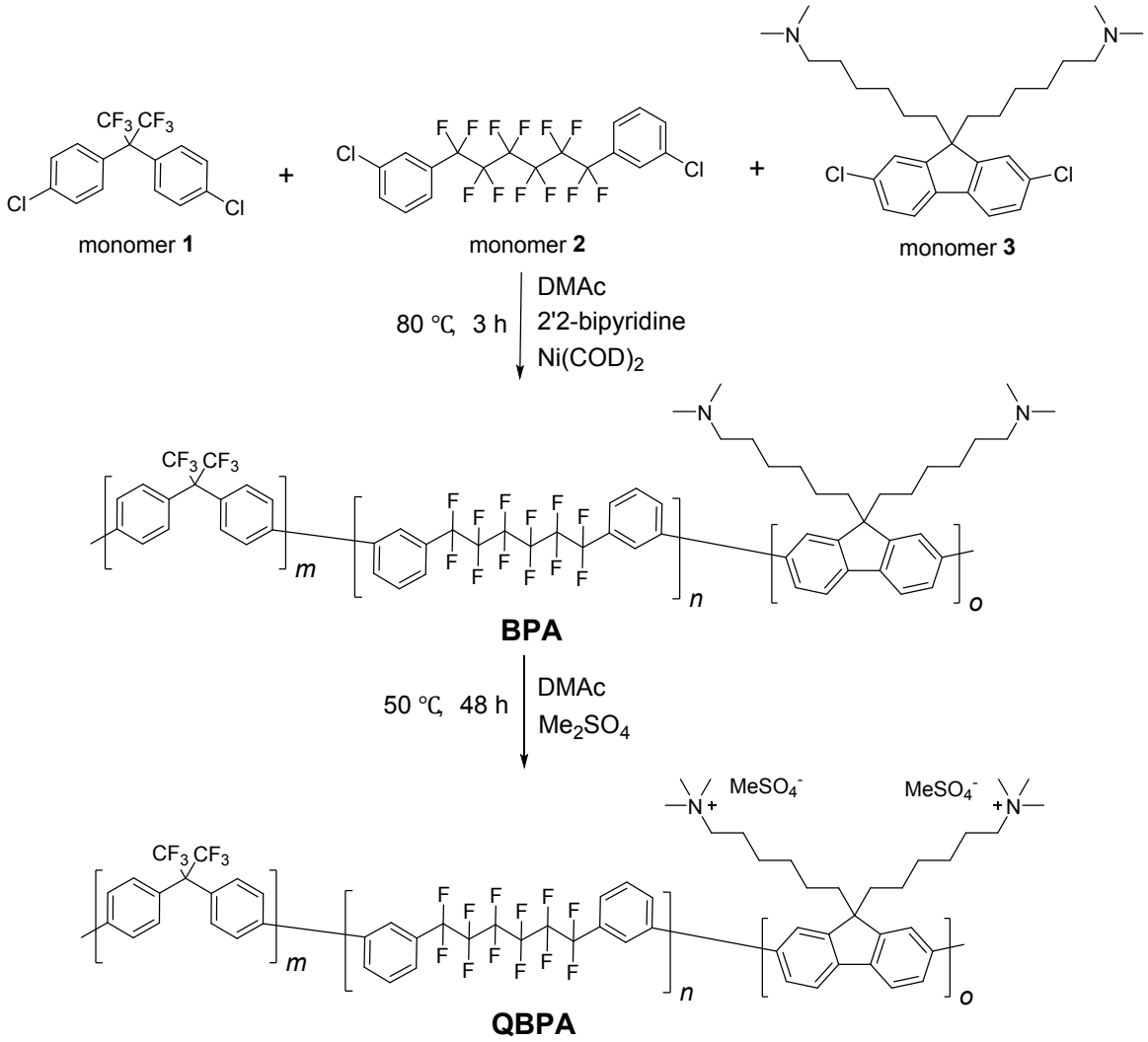

Scheme 4 Synthesis of QBPA.

Table 1. Results of the polymerization and quaternization reactions.

No.	Feed composition			Experimental composition[a]			Molecular weight (kDa)[b]		Yield[c] (%)	IEC[d] (meq. g^{-1})
	m	*n*	*o*	*m*	*n*	*o*	M_n	M_w		
1	1.00	0.20	0.84	1.00	0.20	0.92	8.4	45.3	96	2.11
2	1.00	1.00	1.61	1.00	0.96	1.62	8.0	43.0	98	2.01

3	0.50	0.75	1.04	0.50	0.71	1.01	7.1	41.6	91	2.02
4	0.20	1.00	1.09	0.20	0.99	1.08	7.1	35.2	98	2.11
5	1.00	0.20	1.52	1.00	0.18	1.48	9.4	56.4	96	2.54

[a]Determined from the ^{1}H NMR spectra of the BPA polymers. [b]As BPA analyzed by GPC (calibrated with polystyrene standards). [c]Total yield. [d]IEC determined by titration.

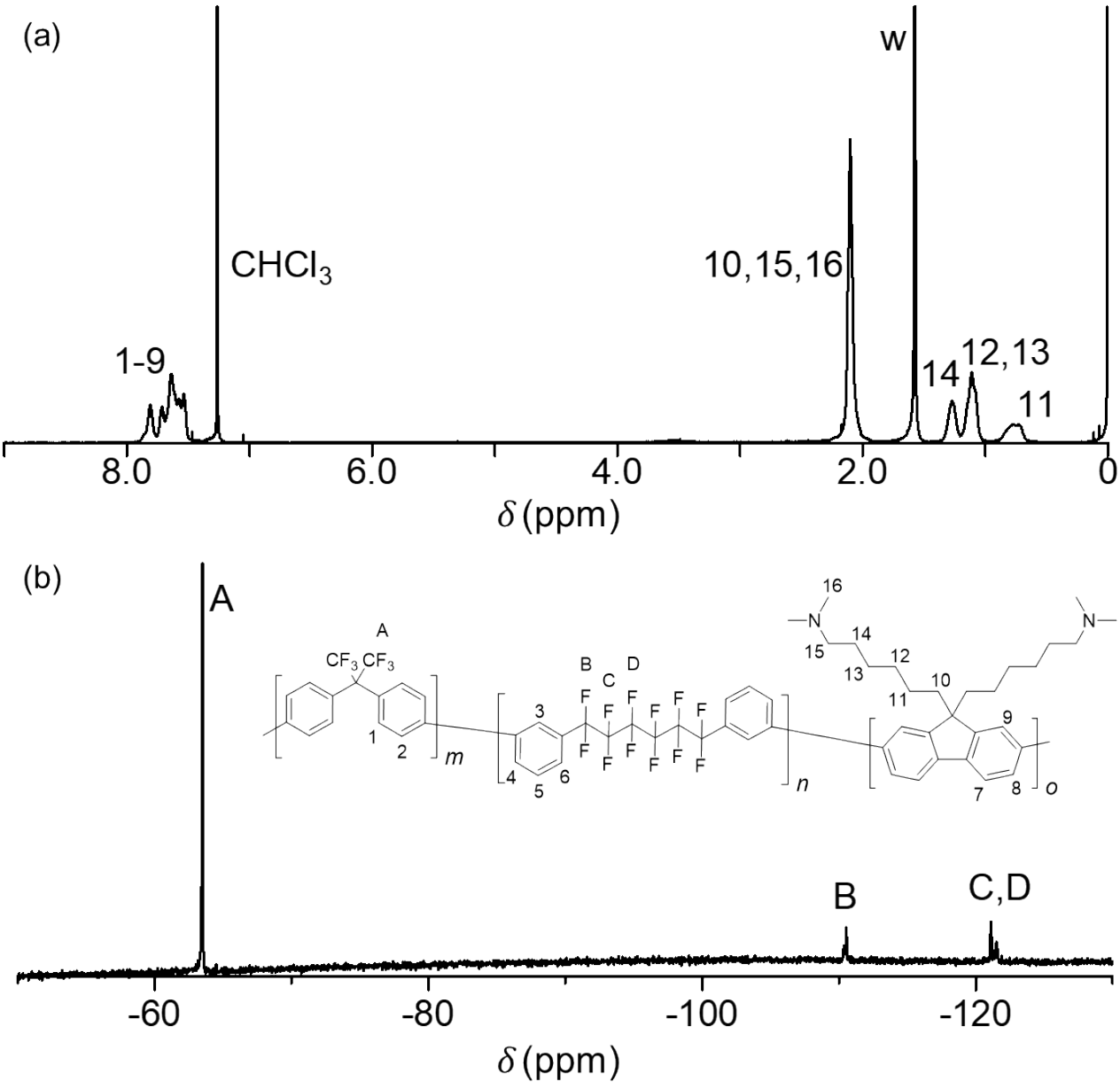

Fig. 2 (a) ^{1}H and (b) ^{19}F NMR spectra of BPA-1 in $CDCl_3$.

QBPA terpolymers were synthesized by quaternization of the precursor BPA with dimethyl sulfate in DMAc (Scheme 4). After the reaction at 50 ºC for 2 days, the products were recovered as pale yellow powder in high yields. Regardless of the compositions, QBPA were soluble in DMAc, DMSO, and methanol, but insoluble in $CHCl_3$ and ethanol. The structure of QBPA was analyzed by ^{1}H and ^{19}F NMR spectra. A typical example is shown in Fig. 3 for QBPA-1 (m/n/o=1.00/0.20/0.84). In the ^{1}H NMR spectrum, methyl proton peak (No. 16) observed at 2.10 ppm for BPA was absent for QBPA. Instead, new peak (No. 16) appeared at 2.93 ppm assignable to methyl protons attached to the quaternary ammonium groups. There were only minor differences in the ^{19}F NMR spectrum between BPA and QBPA. The results suggest that the quaternization reaction was successful without detectable side reactions. Similar results were obtained for QBPAs with other compositions. QBPA membranes were obtained by casting from DMAc solution. The resulting membranes were transparent, light brown, and bendable similar to our previous copolymer membranes having perfluorohexylene (PAF)[16] or hexafluoroisoprolylidene (BAF)[17] groups as hydrophobic components. The IEC values of QBPA membranes were obtained by titration as shown, which were in good accordance with those calculated from the feed compositions (2.10 meq. g^{-1}) within acceptable errors.

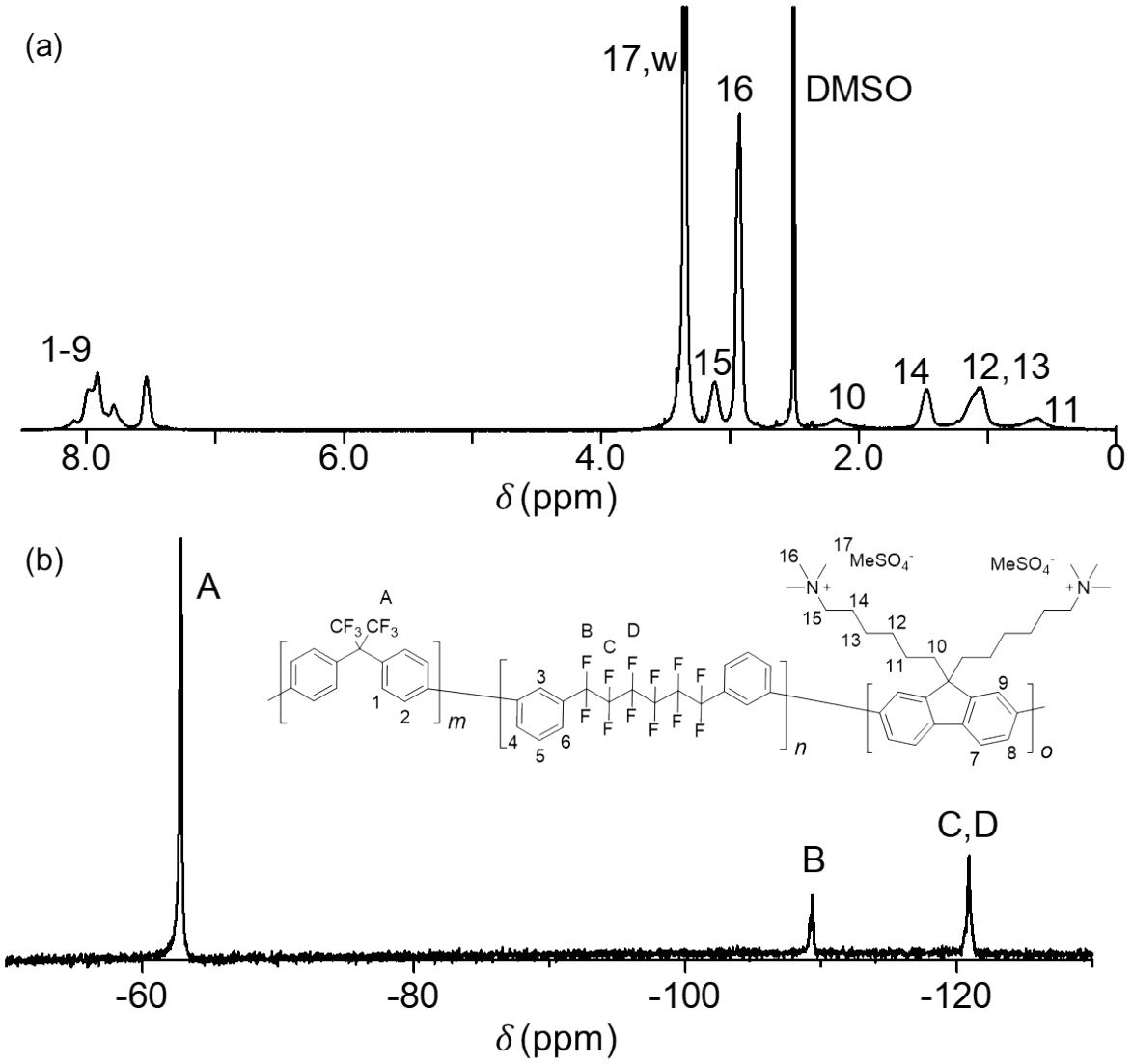

Fig. 3 (a) ^{1}H and (b) ^{19}F NMR spectra of QBPA-1 in DMSO-d_6.

Morphology of QBPA membranes

Fig. 4 shows TEM images of QBPA-1,2,3,4,5 membranes stained with tetrachloroplatinate ($PtCl_4^{2-}$) ions. The dark areas represent ionic clusters containing aggregated ammonium tetrachloroplatinate groups, while the bright areas represent non-ionic domains composed of hydrophobic components. Overall, four membranes exhibited similar phase-separated

morphology. The hydrophilic and hydrophobic domains were both spherical with ca. 2 nm in diameter. The hydrophobic domains were relatively more interconnected. The hydrophobic composition was unlikely to affect the morphology of the membranes. The morphology of QBPAs was similar to that of the parent copolymers QPAF-4[16] and BAF-QAF[17] membranes. QBPA-5 contained slightly more hydrophilic clusters than the other membranes because of larger IEC (higher hydrophilic composition).

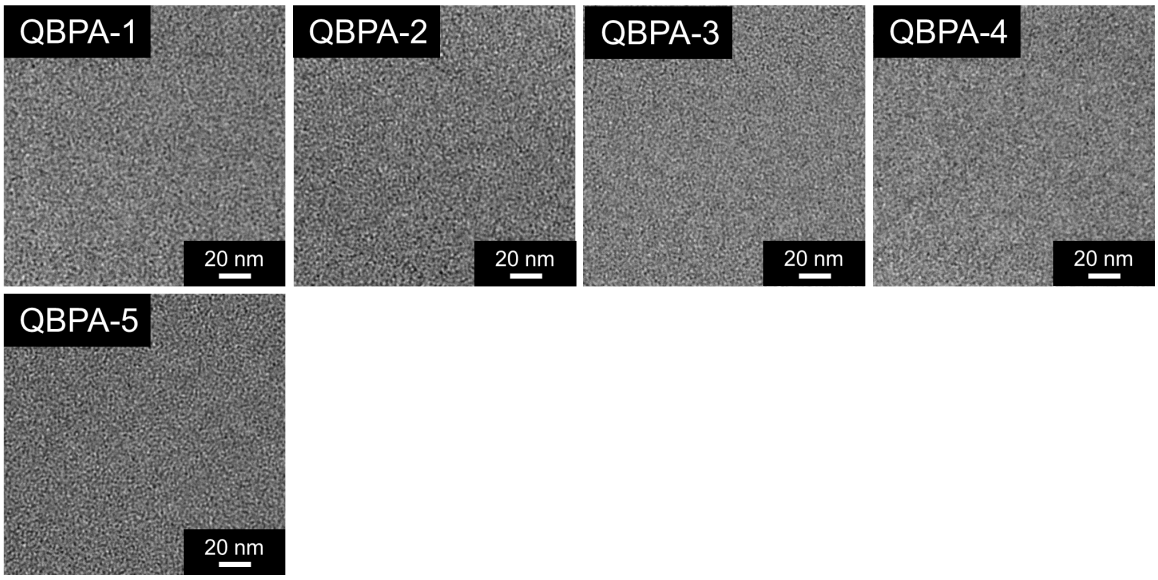

Fig. 4 TEM images of QBPA-1,2,3,4,5 membranes stained with tetrachloroplatinate ions.

SAXS patterns of QBPA membranes (in Cl^- ion forms) were obtained at different relative humidity as shown in Fig. 5. QBPA-1 with the smallest PAF composition did not show peaks and the SAXS patterns were independent on the humidity, similar to BAF-QAF membrane.

As increasing the PAF composition, a peak developed at q = ca. 0.9 nm^{-1} (d = ca. 7 nm) for QBPA-2, q = ca. 0.8 nm^{-1} (d = ca. 8 nm) for QBPA-3 and q = ca. 0.8 nm^{-1} (d = ca. 8 nm) for QBPA-4, respectively. The peak position and intensity did not change with the humidity. In fact, the SAXS pattern of QBPA-4 was similar to that of QPAF-4, which exhibited a peak at q = ca. 0.9 nm^{-1} (d = ca. 7 nm). The results suggest that the periodic structure was more related with the hydrophobic domains associated with the PAF component. QBPA-5 with the same hydrophobic composition as that of QBPA-1 and higher IEC (higher hydrophilic composition) exhibited similar SAXS patters, supporting the idea on the PAF-related periodic hydrophobic domains. Compared to the TEM images where the effect of the PAF composition was not observed, the SAXS patterns revealed the existence of the periodic structure dependent on the composition of the hydrophobic components. It should be noted that the counter ions were different for TEM images ($PtCl_4^{2-}$) and SAXS profiles (Cl^-), which might have affected the phase-separated morphology and its periodicity.

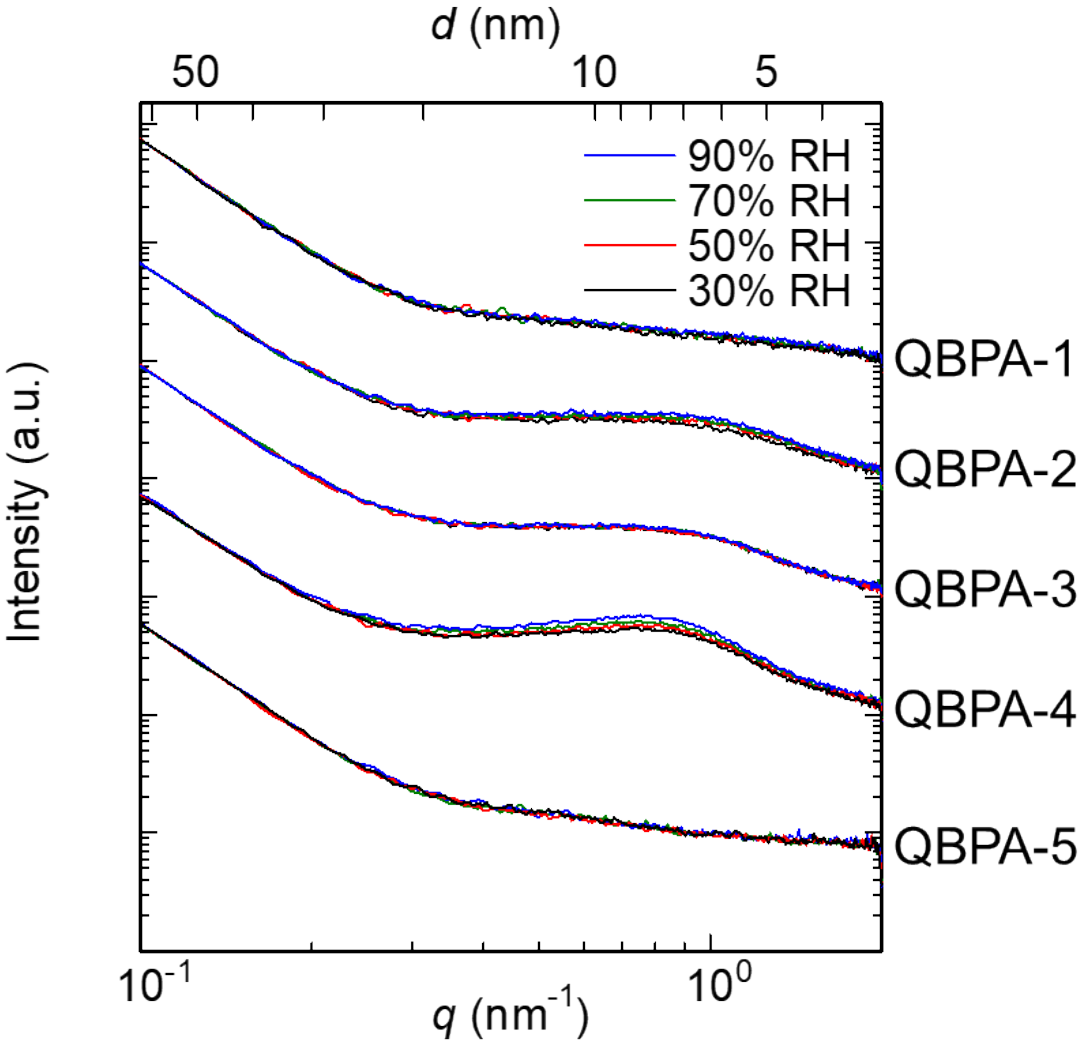

Fig. 5 SAXS profiles of QBPA membranes (in Cl^- forms) as a function of the scattering vector (q) value at 40 ℃.

Water uptake and OH^- conductivity

Water uptake and OH^- conductivity of the QBPA membranes were measured in water (Fig. 6). For comparison, data of BAF-QAF and QPAF-4 membranes with comparable IEC values (1.95-2.11 meq g^{-1}) are also included. Water uptake increased as the PAF composition increased, probably because the perfluoroaliphatic groups were more likely to change the

conformation as absorbing water. The effect was more pronounced when the PAF composition was higher than 80 mol%. QBPA-5 with higher IEC (2.54 meq. g^{-1}) showed 176% of the water uptake, ca. 1.8 times higher than that (99%) of QBPA-1 having the same hydrophobic composition. Different from the water uptake, the ion conductivity exhibited nearly volcano-type dependence on the hydrophobic composition, where the highest conductivity (83 mS cm^{-1}) was obtained with QBPA-2. It is noted that the higher IEC QBPA-5 showed slightly lower conductivity (77 mS cm^{-1}) than that (81 mS cm^{-1}) of QBPA-1 since the higher water absorption lowered practical concentration of the hydroxide ions. The ion conductivity is replotted as a function of IEC_{volume} (volumetric IEC taking the absorbed water into account) in Fig. 7. Apart from QPAF-4 copolymer membrane which showed the lowest IEC_{volume} (due to the largest water absorption) and thus the lowest conductivity, conductivity and its IEC_{volume} dependence of QBPA terpolymers and BAF-QAF copolymer were not well-correlated with the chemical composition. The conductivity did not change much with the IEC_{volume}. BAF-QAF showed rather low conductivity despite its high IEC_{volume}, suggesting that the ion diffusion was slower than the QBPA terpolymers containing PAF component. In fact, the diffusion coefficient of hydroxide ions (calculated from the Nernst-Einstein equation using IEC_{volume}) of BAF-QAF was 1.5×10^{-9} m^2 s^{-1} compared to those of QBPA terpolymers ($2.0 - 3.2 \times 10^{-9}$ m^2 s^{-1}), implying the less inter-connected hydrophilic domains

as ionic pathway. Such differences in the ion diffusion coefficient were also responsible for the volcano-type dependence of the conductivity in Fig. 6.

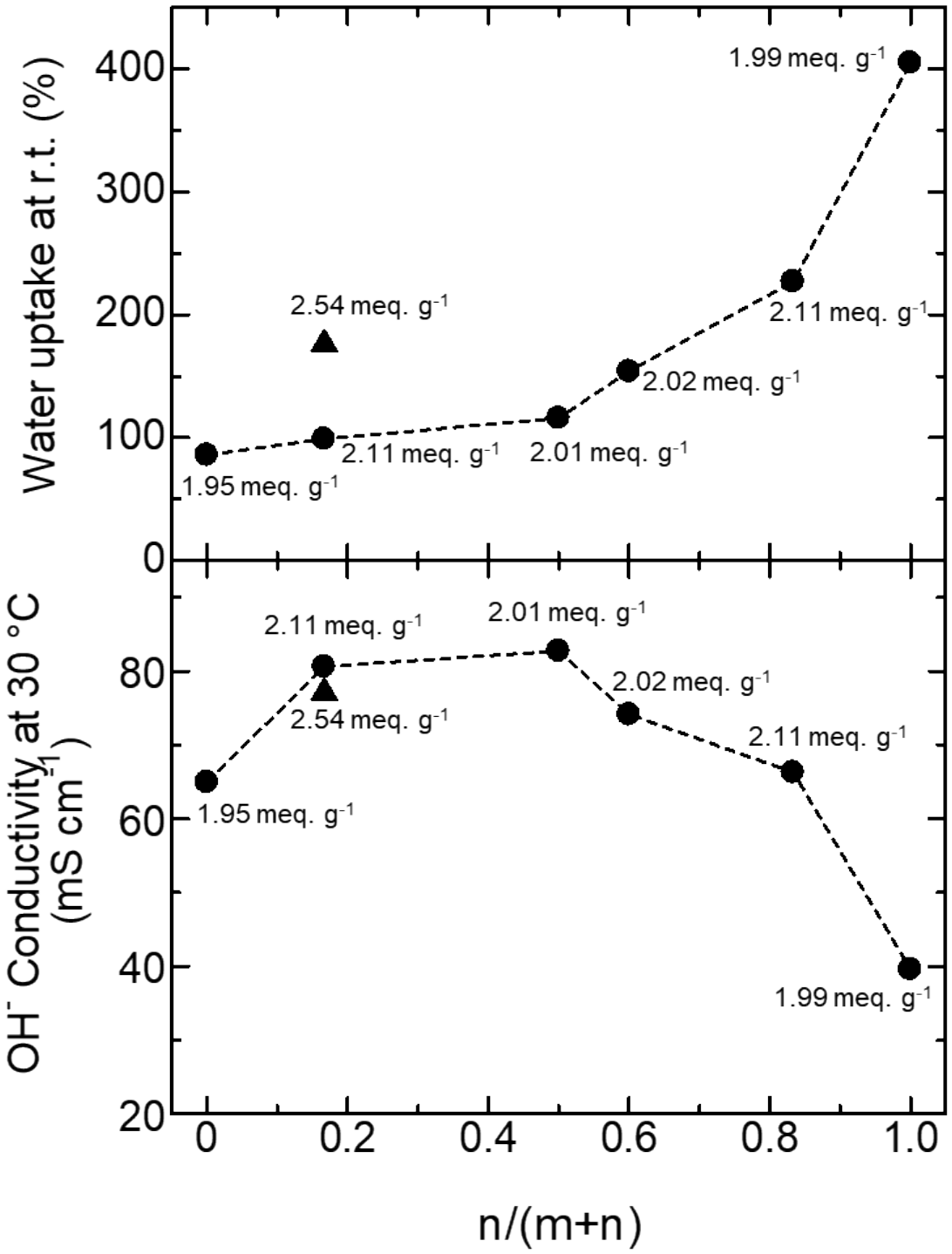

Fig. 6 Water uptake at room temperature and OH^- conductivity at 30 ℃ of QBPA, BAF-QAF, and QPAF-4 membrane as a function of the PAF composition.

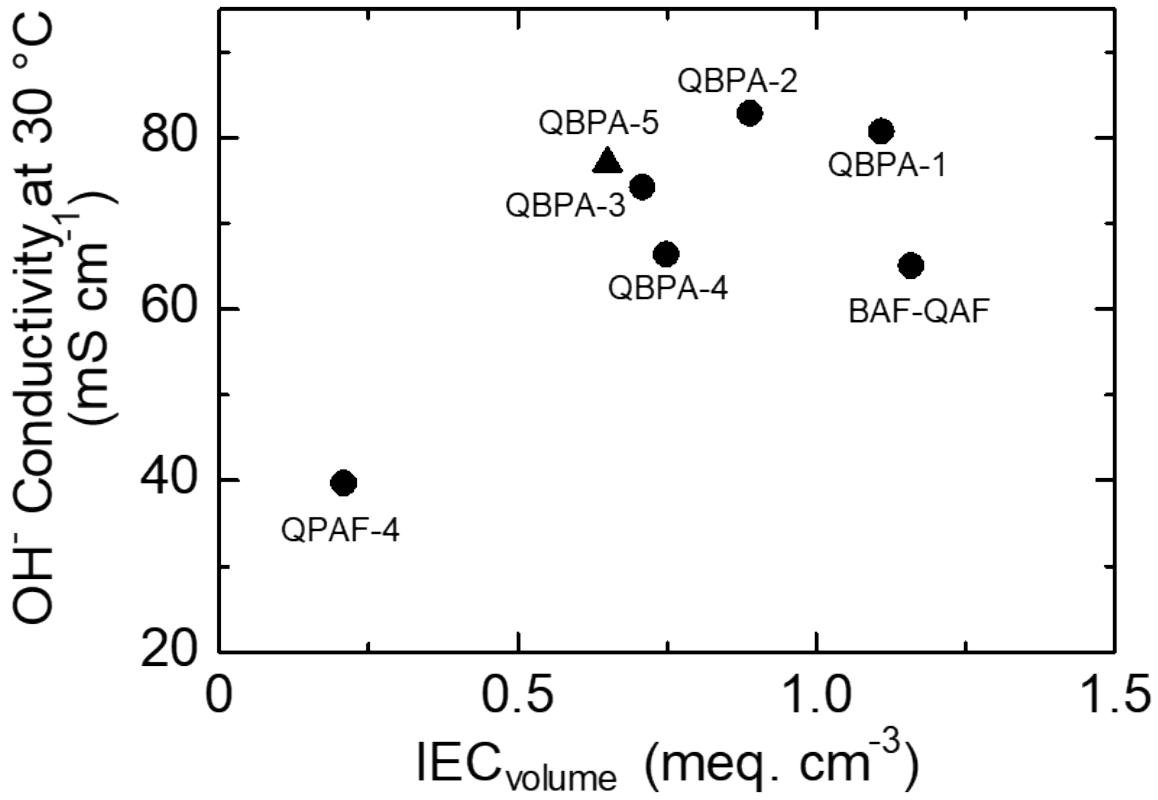

Fig. 7 OH^- conductivity at 30 ℃ of QBPA, BAF-QAF, and QPAF-4 membrane as a function of IEC_{volume}.

Temperature dependence of OH^- conductivity of QBPA, BAF-QAF and QPAF-4 membranes in water is shown in Fig. 8. All membranes showed approximate Arrhenius-type temperature dependence up to 80 ℃. QBPA-1 membrane with IEC = 2.11 meq. g^{-1} achieved the highest conductivity of 161 mS cm^{-1} at 80 ℃, which was among the highest reported for

anion conductive membranes. The apparent activation energy (E_a) was estimated from the slopes to be 9.5 ~ 12.3 kJ mol^{-1}. QBPA-1 and BAF-QAF having the closer hydrophobic composition showed comparable activation energy. Similarly, QBPA-4 and QPAF-4 also showed comparable activation energy. Since QBPA-1 and -5 membranes exhibited similar activation energy, IEC values seemed less relevant. These activation energies fall in the range of the values found in the literature, suggesting the migration of the hydrated hydroxide ions via Grotthuss mechanism.[18,19]

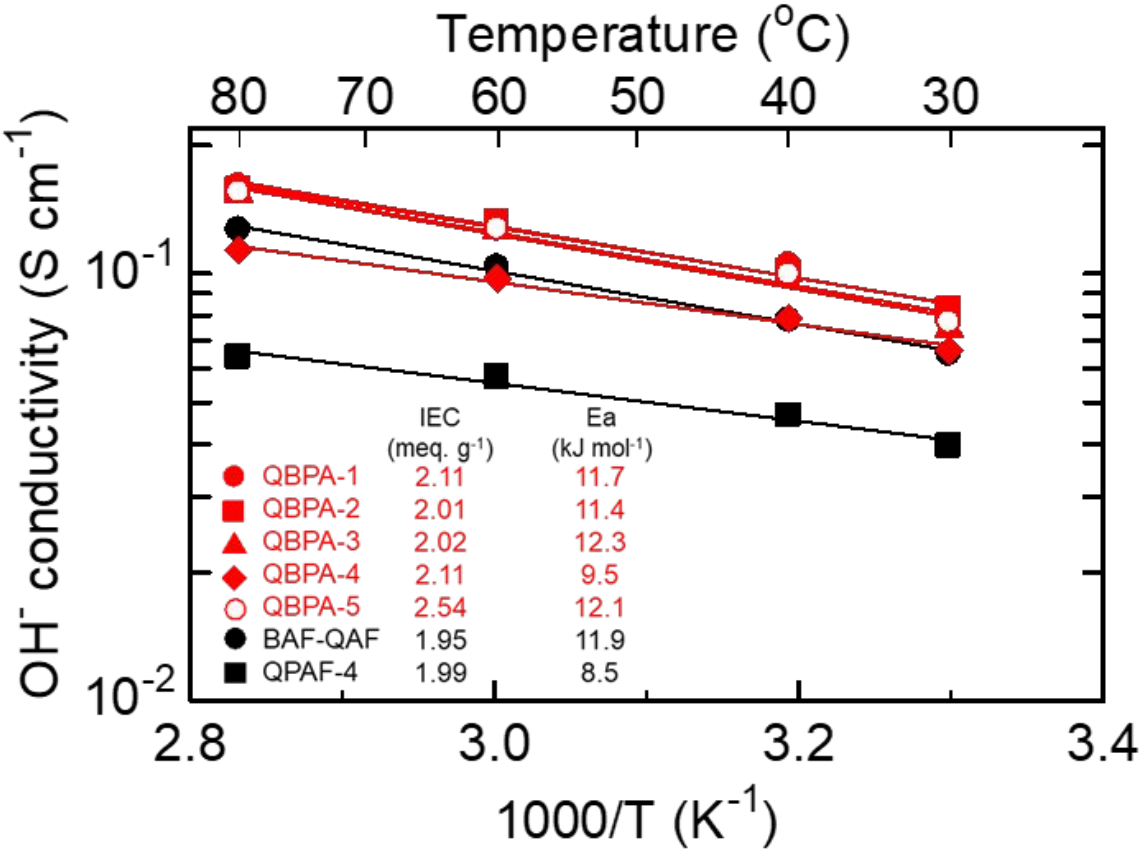

Fig. 8 Temperature dependence of OH$^-$ conductivity of QBPA, BAF-QAF, and QPAF-4 membranes in water.

Mechanical properties

As a mechanical properties test, dynamic mechanical analysis (DMA) was carried out for QBPA-1,2,3,4 membranes in Cl^- forms and compared with BAF-QAF and QPAF-4 membranes. The storage moduli (E'), loss moduli (E"), and tan δ (= E"/E') are shown in Fig. 9 (a) as a function of relative humidity at 80 ºC and (b) as a function of temperature at 60% RH. In the humidity dependence, QBPA membranes showed a slight decrease in E' and E" and no peaks in the tan δ curves similar to the copolymer membranes. The loss in E' was in the order, BAF-QAF < QBPA-1, and -2 < QBPA-3, and -4 < QPAF-4, indicating that PAF components were more responsible to the viscoelastic property and its humidity dependence. In the temperature dependence, QBPA-4 membrane showed a decrease in E' and a broad peak in E" around 90 ºC, similar to QPAF-4 membrane. The results indicate that the T_g was associated with the PAF component and that T_g appeared when the PAF composition was higher than 80 mol%.

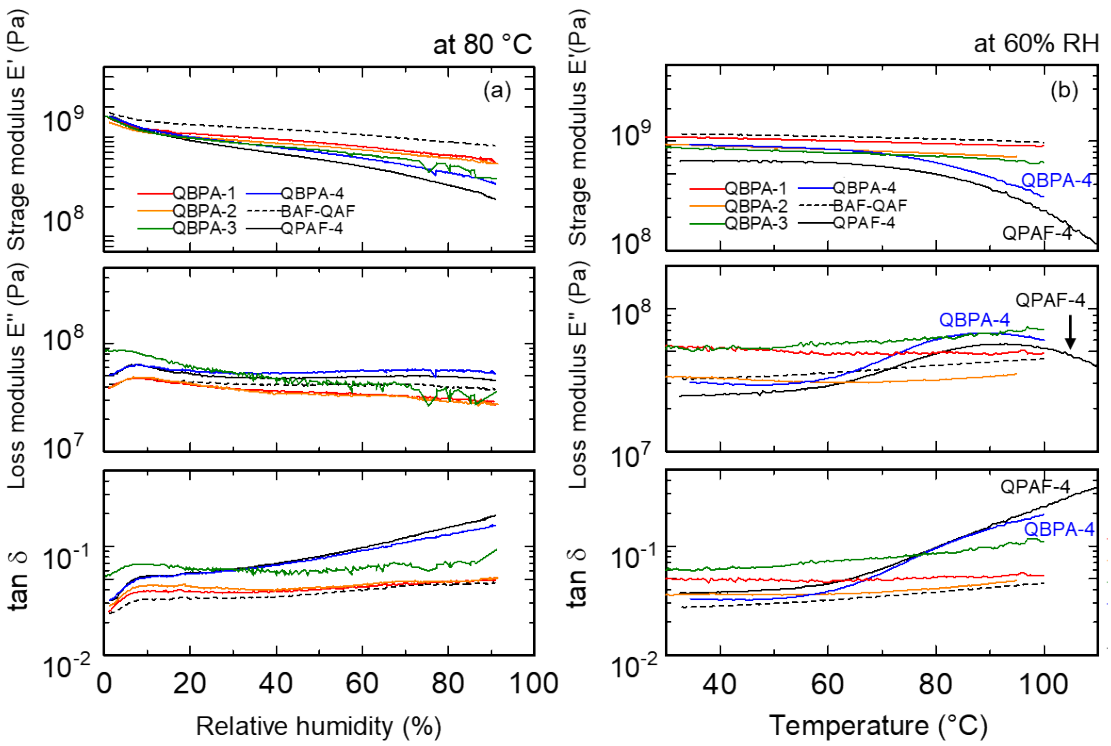

Fig. 9 DMA of QBPA (solid lines), BAF-QAF (dashed line), and QPAF-4 (solid line) membranes in Cl^- forms. (a) Relative humidity dependence at 80 ºC and (b) temperature dependence at 60% RH.

The elongation tests were then carried out for QBPA membranes at 80 ºC and 60% RH (Fig. 10). Data for BAF-QAF and QPAF-4 membrane are also included for comparison. The terpolymer QBPA membranes exhibited stress and strain properties intermediate between BAF-QAF and QPAF-4 copolymer membranes, suggesting that the hydrophobic component impacted on the mechanical properties. Maximum stress, elongation at break, and Young's modulus are plotted as a function of the hydrophobic composition in Fig. 11. There was a distinct trend that as increasing the PAF composition (n/(m+n)), the elongation at break

increased and the maximum stress and Young's modulus declined. The effect seemed more striking at 60-80 mol% of the PAF composition. The PAF as less rigid aliphatic groups than the aromatic BAF groups contributed to increasing the elongation at break. QBPA-5 having higher IEC (2.54 meq g^{-1}) showed higher elongation at break (82%) and comparable maximum stress (21 MPa) and Young's modulus (0.44 GPa) compared to those (47%, 20 MPa, and 0.48 GPa, respectively) of QBPA-1 sharing the same hydrophobic composition. The water molecules might have functioned as plasticizer (water uptake was 99% and 176% for QBPA-1 and -5, respectively, in water at r.t., see Fig. 6). Overall, taking water absorbability, hydroxide ion conductivity, and mechanical properties into account, QBPA-1 and -5 membranes having 17 mol% of the PAF component exhibited the best-balanced properties among those terpolymer and copolymer membranes.

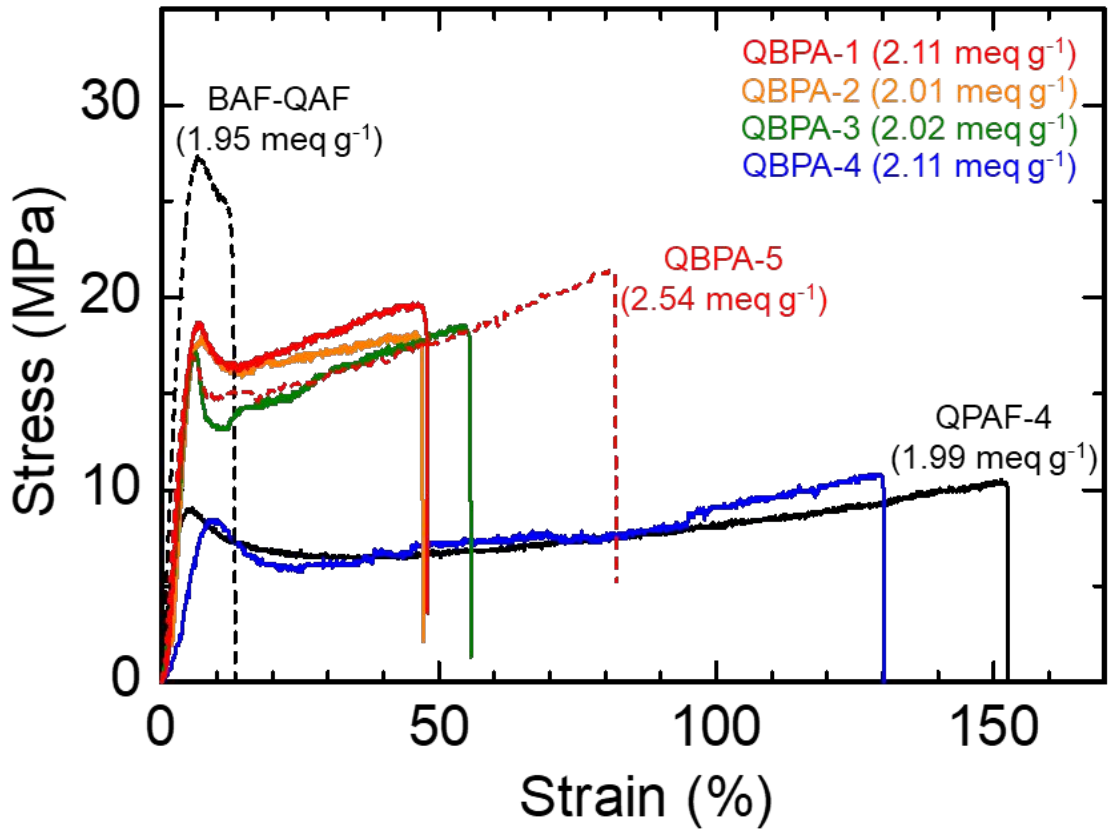

Fig. 10 Stress versus strain curves of QBPA-1,2,3,4 (solid lines), QBPA-5 (dashed line), BAF-QAF (dashed line), and QPAF-4 (solid line) membranes in Cl^- forms at 80 ºC and 60% RH.

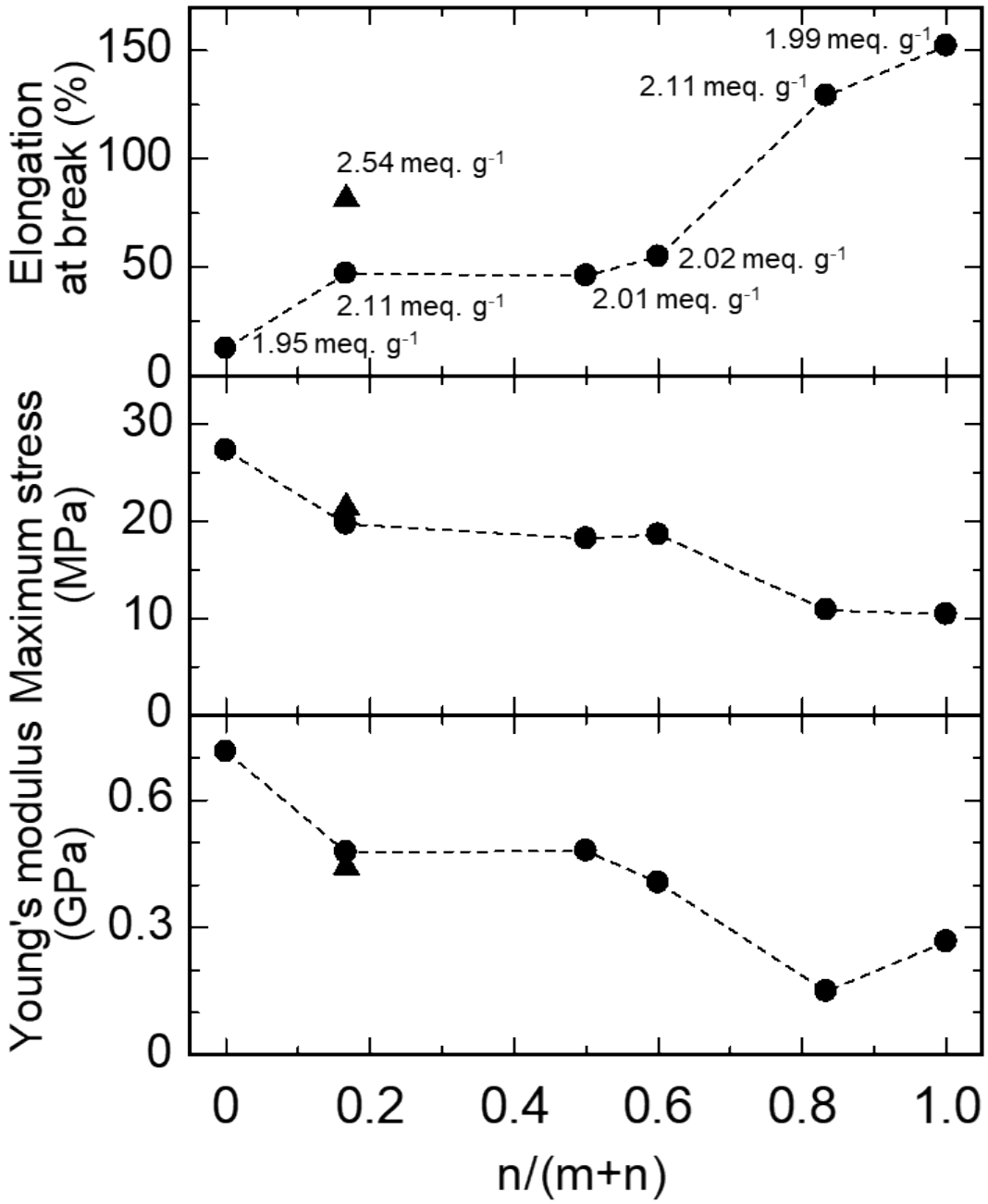

Fig. 11 Mechanical properties of QBPA, BAF-QAF, and QPAF-4 membranes as a function of n/(m+n) in the elongation test.

Alkaline stability

The alkaline stability of the QBPA membranes was tested in 8 M KOH at 80 ºC (Fig. 12). For all terpolymer and copolymer membranes, the conductivity decreased as the testing time. BAF-QAF and QPAF-4 membranes exhibited a decrease in the conductivity from 78 mS cm^{-1} to 12 mS cm^{-1} (16% remaining) and 61 mS cm^{-1} to 20 mS cm^{-1} (33% remaining), respectively. Since the initial conductivity was higher, QBPA membranes retained higher conductivity than 40 mS cm^{-1} even after 1000-hour alkaline stability test. In particular, QBPA-5 with the highest IEC showed 76 mS cm^{-1} of the post-test conductivity with 67% remaining. Then, QBPA-1 membrane was tested under severer conditions in 10 M KOH at 80 ºC (Fig. S1). The conductivity decreased to 30 mS cm^{-1} (32% remaining) after 1000 h and 3 mS cm^{-1} (4% remaining) after 2000 h. The conductivity during the tests is re-plotted as a function of the IEC (varying during the test) in Fig. 13. Regardless of the test conditions, the conductivity was approximately on the same line, indicating that the alkaline degradation of the membranes was most likely related with the decomposition of the ammonium groups in both conditions. Since the post-test membranes retained the shape and bendability (Fig. S2), it is suggested that the polymer main chain was not deteriorated although GPC analyses were not available for the quaternized polymers. The selected membranes (QBPA-1 and -4) were subjected to the stress versus strain tests after the alkaline stability test (Fig. S3). While both membranes showed some changes in the curves (somewhat higher maximum stress for

QBPA-1 and higher yield strain for QBPA-4), the differences were not significant but rather minor. In the ^{1}H NMR spectrum of the post-test QBPA-1 membrane, new peaks appeared at 1.9-2.0 ppm and 4.8-5.7 ppm assignable to dimethylammonium and alkene groups, respectively. The integral ratio of the trimethylammonium protons (peak 16) decreased after the test, and the calculated IEC_{NMR} decreased by 0.4 meq g^{-1} (1.71 meq g^{-1}) compared to the initial IEC_{NMR}. In the ^{19}F NMR spectrum, no practical changes were detected. Those analytical data made us conclude that the alkaline degradation involved Hofmann elimination (a) and the nucleophilic substitution reaction (b, c) on the pendant trimethylammonium groups but not the main chain decomposition (Fig. 15).

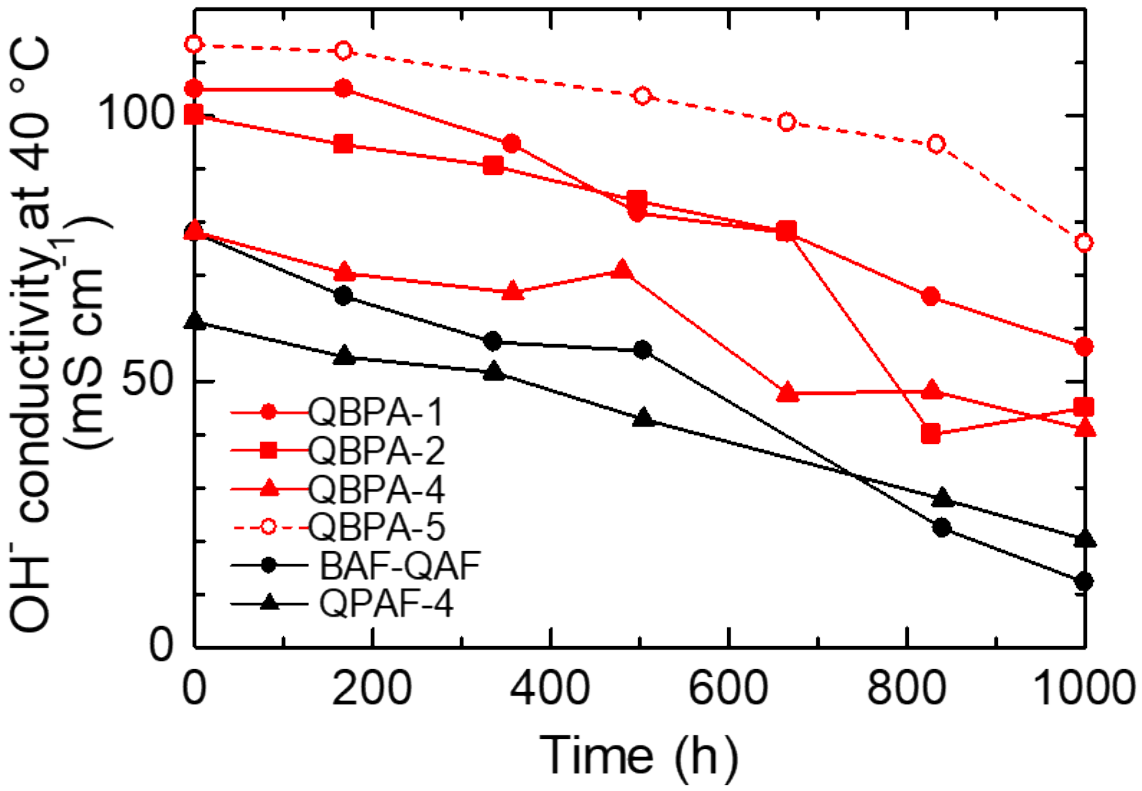

Fig. 12 Time course of the hydroxide ion conductivity of QBPA, BAF-QAF, and QPAF-4 membranes in 8 M KOH aqueous solution at 80 ℃.

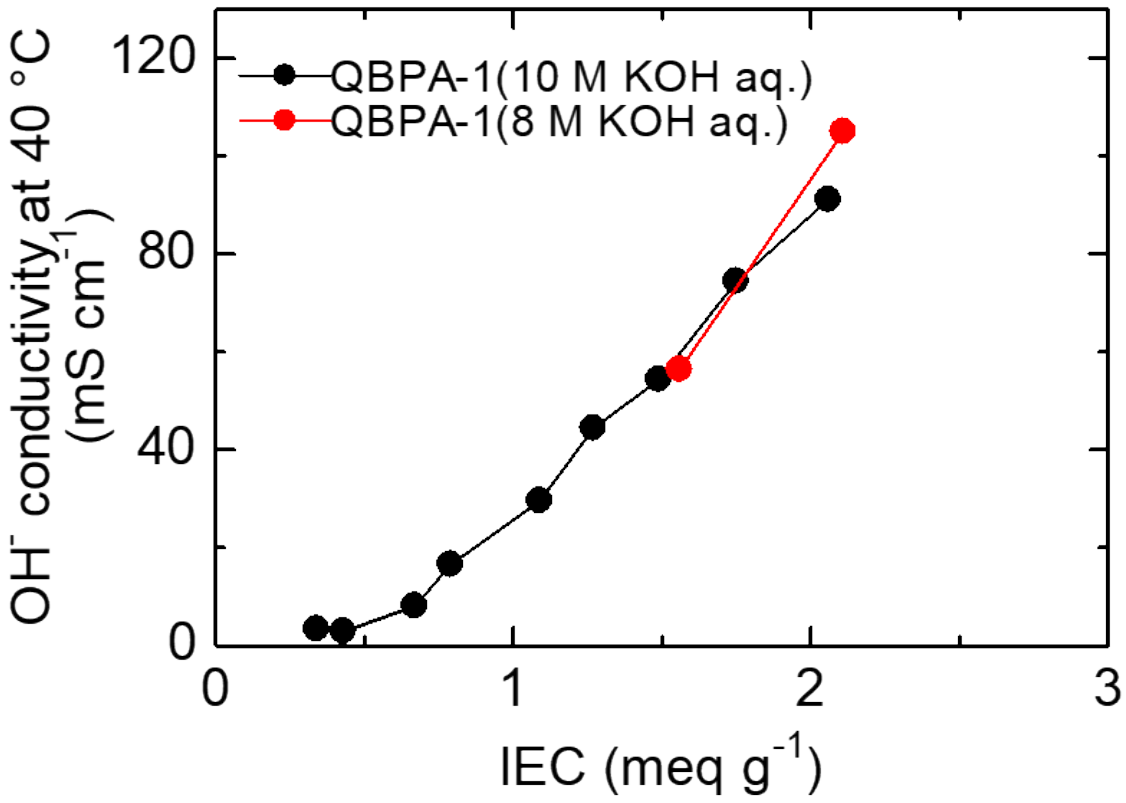

Fig. 13 Hydroxide ion conductivity of QBPA-1 membrane during 8 M and 10 M KOH stability test as a function of IEC.

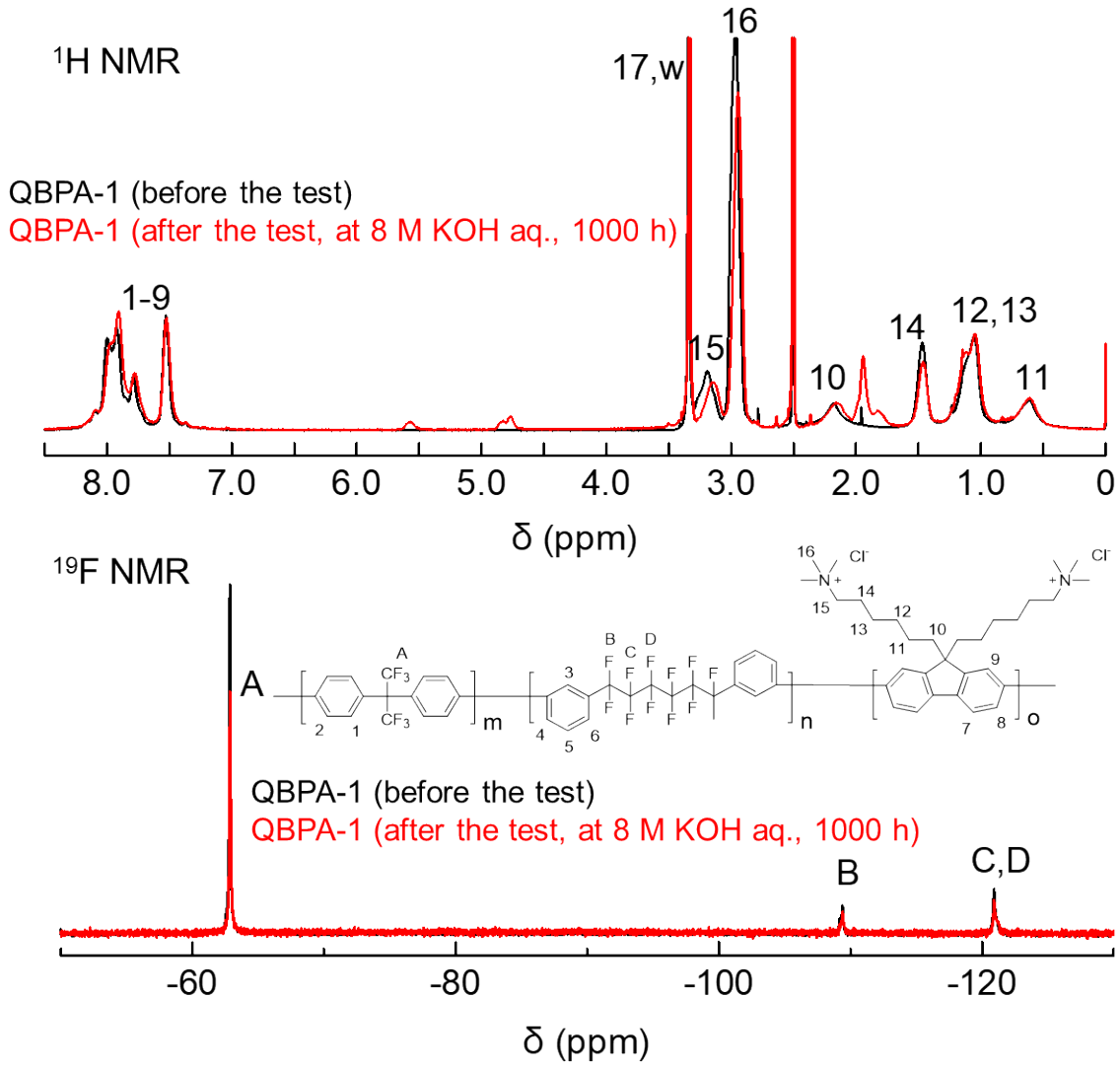

Fig. 14 ^{1}H and ^{19}F NMR spectra of QBPA-1 before (black line) and after (red line) the 8 M KOH stability test in Cl^- form membranes (IEC = 1.56 meq g^{-1}) in DMSO-d_6.

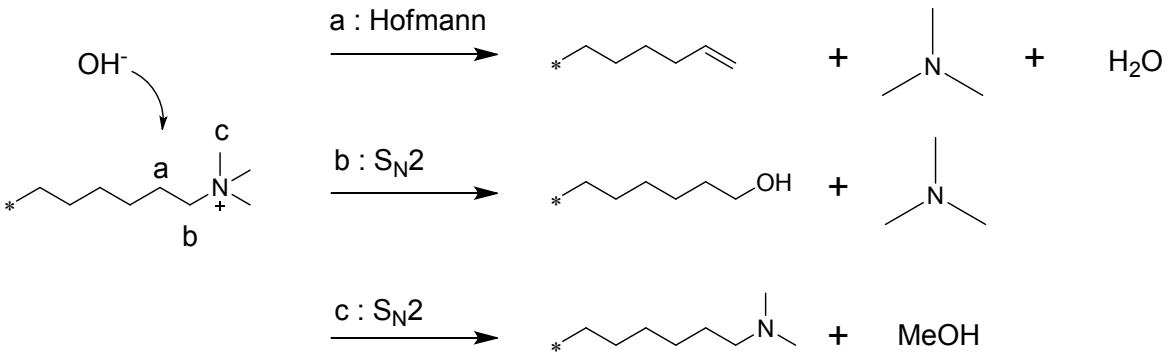

Fig. 15 Possible decomposition mechanisms of trimethylammonium groups by hydroxide ions.

Gas permeability

Hydrogen and oxygen gas permeability of QBPA membranes (in $MeSO_4^-$ forms) were measured at 80 ºC and 0% RH and plotted as a function of the PAF composition in Fig. 16. For comparison, data for BAF-QAF and QPAF-4 (both in $MeSO_4^-$ forms) membranes are also included. The gas permeability coefficient, both of hydrogen and oxygen, exhibited minor dependence on the PAF composition with the smallest for QBPA-4 membrane (1.10×10^{-9} cm^3(STP) cm s^{-1} cm^{-2} $cmHg^{-1}$ for hydrogen and 8.63×10^{-11} cm^3(STP) cm s^{-1} cm^{-2} $cmHg^{-1}$ for oxygen, respectively). Assuming that hydrophobic domains were more responsible for the gas permeation at least under dry conditions, the smallest gas permeability coefficient of QBPA-4 membrane must be related with more developed hydrophobic domains with periodicity (as discussed above with the SAXS data). It is noticeable that the differences in the permeability coefficient between hydrogen and oxygen

(ca. one order of magnitude for all membranes, regardless of the PAF composition) were the results of differences in the diffusion coefficients. In fact, the differences in the solubility coefficients between hydrogen and oxygen were rather minor (ca. 1.1 - 1.4 times). The partially fluorinated hydrophobic components must have affinity to oxygen molecules resulting in the increased solubility coefficient.

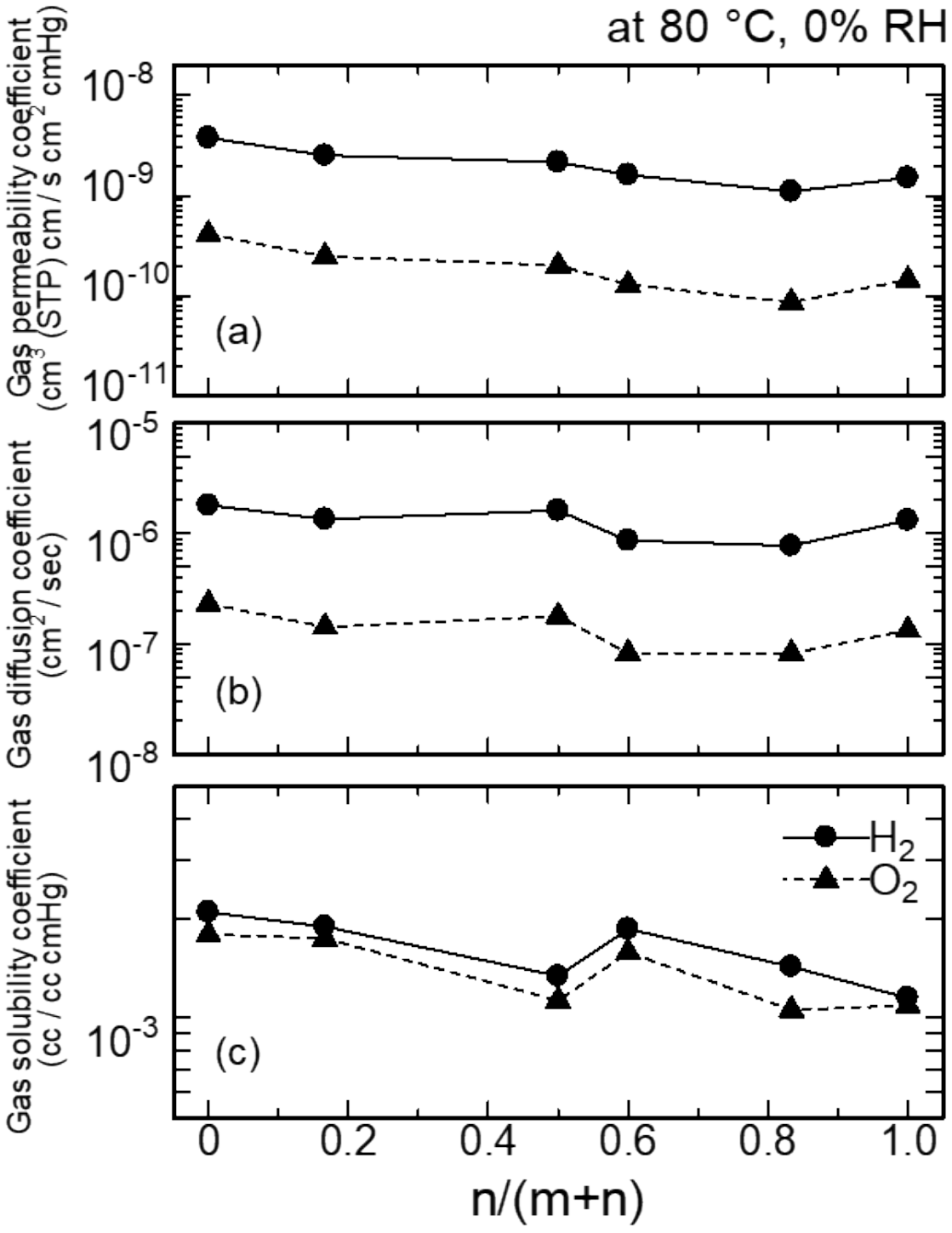

Fig. 16 Hydrogen (circle) and oxygen (triangle) (a) permeability coefficient, (b) diffusion coefficient, and (c) solubility coefficient of QBPA, BAF-QAF, and QPAF-4 membranes at 80 ℃ as a function of the PAF composition.

Fuel cell performance

Taking the total properties into account, QBPA-1 containing 17 mol% PAF seemed the best-balanced membranes. For this reason, QBPA-1 membrane was chosen for hydrogen/oxygen fuel cell evaluation. The current density / voltage (I/V) and current density / power density (I/W) curves of an MEA using QBPA-1, BAF-QAF, and QPAF-4 membranes are shown in Fig. 17. The open circuit voltage (OCV) of QBPA-1 cell was 0.94 V, which was comparable to that (ca. 1.0 V) of MEA with BAF-QAF and QPAF-4 membranes with comparable thickness, supporting that all those membranes had low hydrogen permeability. The ohmic resistance of QBPA-1 cell was nearly constant (ca. 0.12 Ω cm^2) and smaller than those of BAF-QAF and QPAF-4 cells at any current density (Fig. 18). The lower ohmic resistance of QBPA-1 cell was the result of higher hydroxide ion conductivity (131 mS cm^{-1} at 60 ºC in water, see Fig. 8) than those of BAF-QAF (104 mS cm^{-1}) and QPAF-4 (58 mS cm^{-1}). QBPA-1 cell exhibited the maximum power density of 273 mW cm^{-2} at the current density of 0.76 A cm^{-2} similar to QPAF-4 and much higher than that (185 mW cm^{-2}) of BAF-QAF cell. Slightly lower performance of QBPA-1 cell than QPAF-4 cell presumably stemmed from the smaller water diffusivity of the membrane (or smaller water back diffusion from the cathode to the anode) causing the lower anodic performance. The maximum power density obtained in the present study was not state-of-the-art compared to the literature works. It

should be noted, however, that Pt loading amount was substantially low (0.2 mg cm^{-2}) and no back pressure was applied for hydrogen and oxygen supply in the present study.

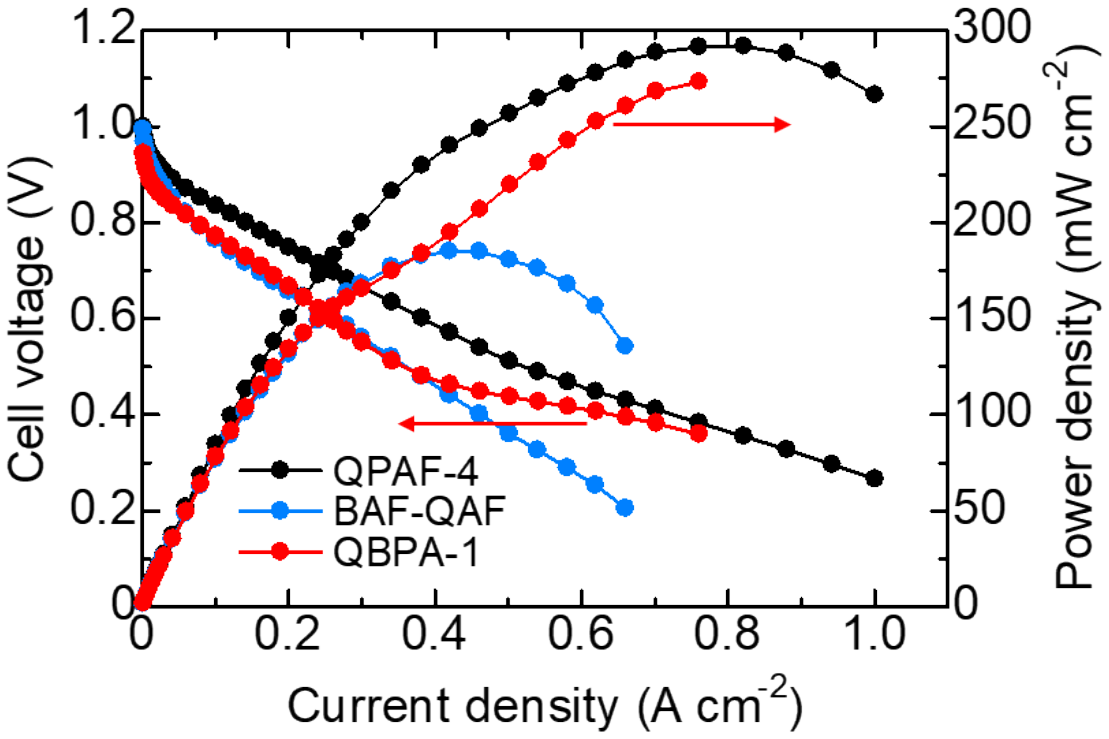

Fig. 17 Fuel cell performance of MEAs using QBPA-1 (red), BAF-QAF (blue) and QPAF-4 (black) as membrane and QPAF-4 as electrode binder at 60 ℃ and 100% RH.

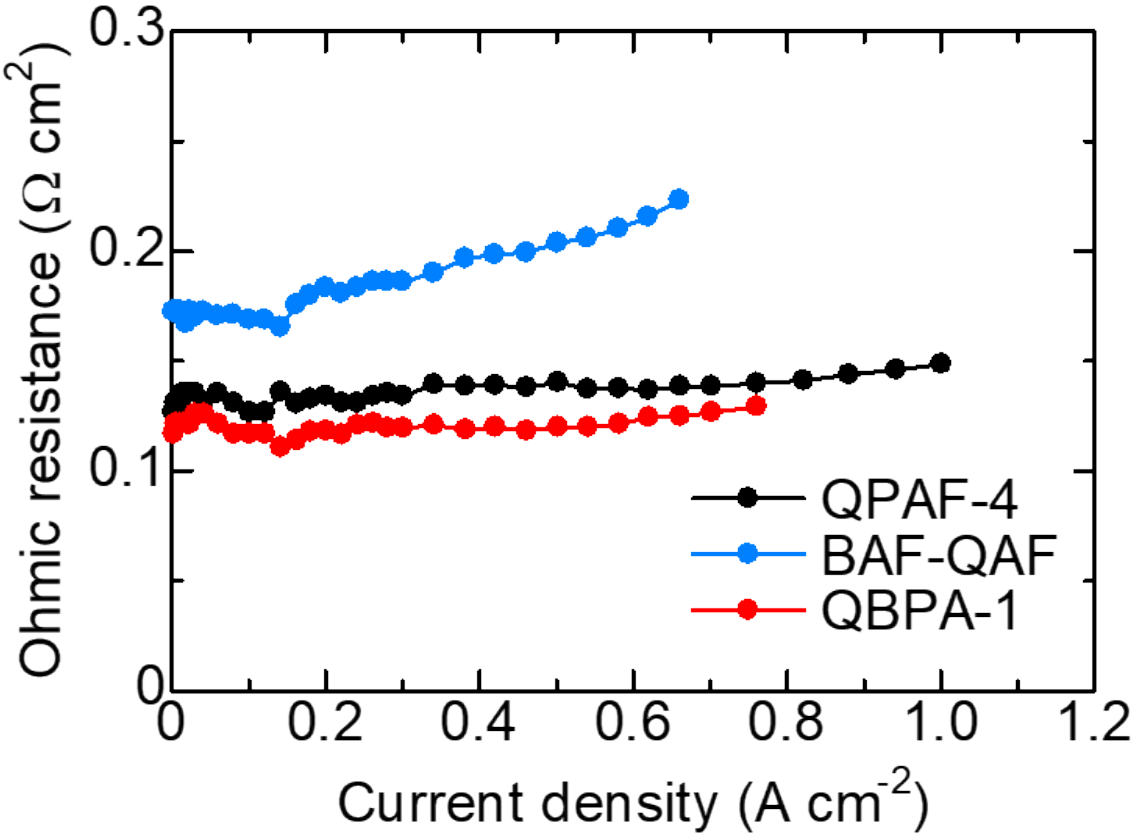

Fig. 18 Ohmic resistance of MEAs using QBPA-1 (red), BAF-QAF (blue) and QPAF-4 (black) as membrane and QPAF-4 as electrode binder at 60 ℃ and 100% RH.

Conclusions

A series of partially fluorinated terpolymers containing perfluorohexylene (PAF) and hexafluoroisopropyridene (BAF) groups as hydrophobic components were synthesized, and effect of the hydrophobic composition on the membrane properties was investigated. While the phase-separated morphology based on the hydrophilic/hydrophobic differences in the polymer components was not much affected as suggested by TEM images and SAXS profiles, water absorbability of the terpolymer membranes was between those of the parent

copolymer membranes and changed as the hydrophobic composition. Similarly, the mechanical properties (elongation at break, maximum stress, and Young's modulus) evaluated by stress versus strain curves and gas barrier properties of the terpolymer membranes appeared between those of the copolymer membranes. The most striking effect was confirmed in the hydroxide ion conductivity, and the maximum conductivity was obtained at 17 - 50 mol% of the PAF composition among the terpolymer membranes containing the similar bulk IEC values, reflecting high ion diffusion and small water absorption. The terpolymer membranes were chemically stable in hot conc. KOH, retaining reasonable ion conductivity after 1000 h, and the alkaline degradation was more related with the ammonium head groups rather than the hydrophobic groups and composition. Hydrogen / oxygen fuel cell was operated using the selected membrane. High OCV and low ohmic resistance were indicative of low gas permeability and high ion conductivity, respectively, confirming the benefit of the terpolymer membrane. For higher alkaline fuel cell performance, however, through-plane water diffusivity needs to be improved[20], which is in our future agenda.

Conflicts of interest

There are no conflicts to declare.

Author contributions

Yoshihiro Ozawa: Investigation, writing

Yuto Shirase: Investigation

Kanji Otsuji: Investigation

Kenji Miyatake: Supervision, writing, reviewing and editing, funding acquisition, and project administration

Acknowledgments

This work was partly supported by the New Energy and Industrial Technology Development Organization (NEDO), the Ministry of Education, Culture, Sports, Science and Technology (MEXT), Japan, through Grants-in-Aid for Scientific Research (18H05515), Japan Science and Technology (JST) through SICORP (JPMJSC18H8), JKA promotion funds from AUTORACE, Iwatani Naoji Foundation, and the thermal and electric energy technology foundation. We thank Tosoh Fine Chem for kindly supplying 1,6-diiodoperfluorohexane.

Notes and References

1 D. R. Dekel, *J. Power Sources*, 2018, **375**, 158-169.

2 W. E. Mustain, M. Chatenet, M. Page and Y. S. Kim, *Energy Environ. Sci.*, 2020, **13**, 2805-2838.

3 N. Chen and Y. M. Lee, *Prog. Polym. Sci.*, 2021, **113**, 101345.

4 R. He, P. Wen, H. N. Zhang, S. Guan, G. Xie, L. Z. Li, M. H. Lee and X. D. Li, *J. Membr. Sci.*, 2018, **556**, 73-84.

5 L. Wang, M. Bellini, H. A. Miller and J. R. Varcoe, *J. Mater. Chem. A*, 2018, **6**, 15404.

6 M. G. Marino and K. D. Kreuer, *ChemSusChem*, 2015, **8**, 513-523.

7 W. You, K. J. T. Noonan and G. W. Coates, *Prog. Polym. Sci.*, 2020, **100**, 101177.

8 N. Chen, C. Long, Y. Li, C. Lu and H. Zhu, *ACS Appl. Mater. Interfaces*, 2018, **10**, 15720-15732.

9 J. Wang, J. Wang, S. Li and S. Zhang, *J. Membr. Sci.*, 2011, **368**, 246-253.

10 C. Fujimoto, D. S. Kim, M. Hibbs, D. Wrobleski and Y. S. Kim, *J. Membr. Sci.*, 2012, **423-424**, 438-449.

11 J. Fan, S. W. Cohen, E. M. Schibli, Z. Paula, W. Li, T. J. G. Skalski, A. T. Sergeenko, A. Hohenadel, B. J. Frisken, E. Magliocca, W. E. Mustain, C. E. Diesendruck, D. R. Dekel and S. Holdcroft, *Nat. Commun.*, 2019, **10**, 2306.

12 Q. Ge, X. Liang, L. Ding, J. Hou, J. Miao, B. Wu, Z. Yang and T. Xu, *J. Mater. Chem. A*, 2016, **4**, 13938-13948.

13 F. H. Zhai, Q. Q. Zhan, Y. F. Yang, N. Y. Ye, R. Y. Wan, J. Wang, S. Chen and R. H. He, *J. Membr. Sci.*, 2022, **642**, 119983.

14 W. Chen, M. Mandal, G. Huang, X. Wu, G. He and P. A. Kohl, *ACS Appl. Energy*

Mater., 2019, **2**, 2458-2468.

15 J. Miyake and K. Miyatake, *Sustain. Energy Fuels*, 2019, **3**, 1916-1928.

16 H. Ono, T. Kimura, A. Takano, K. Asazawa, J. Miyake, J. Inukai and K. Miyatake, *J. Mater. Chem. A*, 2017, **5**, 24804-24812.

17 T. Kimura, A. Matsumoto, J. Inukai and K. Miyatake, *ACS Appl. Energy Mater.*, 2020, **3**, 469–477.

18 Y. Zhou, J. Yang, H. Su, J. Zeng, S. P. Jiang and W. A. Goddard, *J. Am. Chem. Soc.*, 2014, **136**, 4954–4964.

19 A. Ouadah, H. Xu, T. Luo, S. Gao, Z. Zhang, Z. Li and C. Zhu, *RSC Adv.*, 2017, **7**, 47806.

20 K. Otsuji, Y. Shirase, T. Asakawa, N. Yokota, K. Nagase, W. Xu, P. Song, S. Wang, D. A. Tryk, K. Kakinuma, J. Inukai, K. Miyatake, M. Uchida, *J. Power Sources*, 2022, **522**, 230997.